Purdue University
Purdue e-Pubs

Birck and NCN Publications | Birck Nanotechnology Center

5-14-2014

Understanding the Mechanical Properties of DNA Origami Tiles and Controlling the Kinetics of Their Folding and Unfolding Reconfiguration

Haorong Chen
Purdue University, Birck Nanotechnology Center, hrchen@purdue.edu

Te-Wei Wang
Purdue University, Birck Nanotechnology Center, wengt@purdue.edu

Molly M. Riccitelli
Purdue University, Birck Nanotechnology Center, mriccite@purdue.edu

Yi Cui
Purdue University, Bindley Bioscience Center, cui19@purdue.edu

Joseph Irudayaraj
Purdue University, Birck Nanotechnology Center, Bindley Bioscience Center, josephi@purdue.edu

See next page for additional authors

Follow this and additional works at: http://docs.lib.purdue.edu/nanopub

 Part of the Nanoscience and Nanotechnology Commons

Chen, Haorong; Wang, Te-Wei; Riccitelli, Molly M.; Cui, Yi; Irudayaraj, Joseph; and Choi, Jong Hyun, "Understanding the Mechanical Properties of DNA Origami Tiles and Controlling the Kinetics of Their Folding and Unfolding Reconfiguration" (2014). *Birck and NCN Publications.* Paper 1634.
http://dx.doi.org/10.1021/ja500612d

This document has been made available through Purdue e-Pubs, a service of the Purdue University Libraries. Please contact epubs@purdue.edu for additional information.

Authors
Haorong Chen, Te-Wei Wang, Molly M. Riccitelli, Yi Cui, Joseph Irudayaraj, and Jong Hyun Choi

This article is available at Purdue e-Pubs: http://docs.lib.purdue.edu/nanopub/1634

JACS
JOURNAL OF THE AMERICAN CHEMICAL SOCIETY

Article

pubs.acs.org/JACS

Understanding the Mechanical Properties of DNA Origami Tiles and Controlling the Kinetics of Their Folding and Unfolding Reconfiguration

Haorong Chen,[†] Te-Wei Weng,[†] Molly M. Riccitelli,[†] Yi Cui,[‡] Joseph Irudayaraj,[†,‡] and Jong Hyun Choi*,[†]

[†]School of Mechanical Engineering, Birck Nanotechnology Center, Bindley Bioscience Center, Purdue University, West Lafayette, Indiana 47907, United States

[‡]Department of Agricultural and Biological Engineering, Bindley Bioscience Center, Purdue University, West Lafayette, Indiana 47907, United States

Supporting Information

ABSTRACT: DNA origami represents a class of highly programmable macromolecules that can go through conformational changes in response to external signals. Here we show that a two-dimensional origami rectangle can be effectively folded into a short, cylindrical tube by connecting the two opposite edges through the hybridization of linker strands and that this process can be efficiently reversed via toehold-mediated strand displacement. The reconfiguration kinetics was experimentally studied as a function of incubation temperature, initial origami concentration, missing staples, and origami geometry. A kinetic model was developed by introducing the *j* factor to describe the reaction rates in the cyclization process. We found that the cyclization efficiency (*j* factor) increases sharply with temperature and depends strongly on the structural flexibility and geometry. A simple mechanical model was used to correlate the observed cyclization efficiency with origami structure details. The mechanical analysis suggests two sources of the energy barrier for DNA origami folding: overcoming global twisting and bending the structure into a circular conformation. It also provides the first semiquantitative estimation of the rigidity of DNA interhelix crossovers, an essential element in structural DNA nanotechnology. This work demonstrates efficient DNA origami reconfiguration, advances our understanding of the dynamics and mechanical properties of self-assembled DNA structures, and should be valuable to the field of DNA nanotechnology.

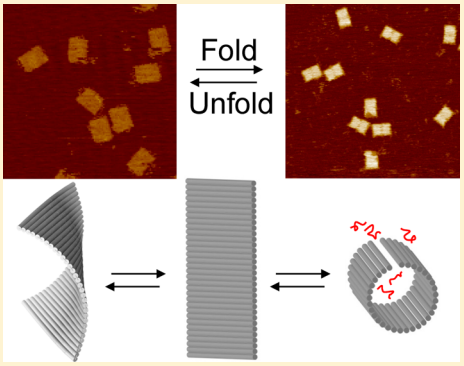

INTRODUCTION

The DNA origami technique has emerged as a powerful method to synthesize programmable nanostructures with high precision.[1−4] This method has created novel structures not only as static templates for organizing functional molecules[5−7] and nanoparticles[8−13] but also as dynamic platforms for sensing and actuation at the nanoscale. Several strategies have been developed to achieve such dynamic, shape-changing origami structures. For instance, origami boxes[14] or clamlike switches[15] that can open in response to external stimuli and molecular forceps[16] that pinch upon binding to a molecular target have been demonstrated. These nanomechanical devices achieve conformation changes by using single-stranded hinges to connect moving parts while treating double-stranded domains as rigid bodies. Reconfiguration can also be achieved via a release-and-reassemble strategy. A hierarchically assembled DNA tube has been shown to switch between different chiralities,[17] and a simple origami structure can be switched into and back from a quasi-fractal pattern.[18]

Recently, rectangular DNA origami sheets densely functionalized with gold nanoparticles were shown to readily roll up into short tubes upon addition of a linker set that connect the two opposite edges.[19] The rolling up of unfunctionalized origami rectangles was also briefly mentioned in the same work. These results suggest that completely base-paired single-layer DNA origami has considerable flexibility that may be used as a new mechanism for dynamic reconfiguration.

In order to explore this possibility, the kinetics of this shape-changing mechanism is systematically studied here. Our model system is an origami tile that globally bends over and seals into a short tube. Unlike most other dynamic DNA structures, the deformation is distributed across the whole sheet instead of being localized at a few single-stranded hinges. We find that the folding kinetics and final yield strongly depend on the incubation temperature, missing staples, and the dimension of the rectangular structure. Elevating the incubation temperature or eliminating as few as seven staples allows folding yields of over 90% to be achieved within 1 h. We also demonstrate that the folding process can be reversed by disengaging the linkers via

Received: January 24, 2014
Published: April 21, 2014

 © 2014 American Chemical Society dx.doi.org/10.1021/ja500612d | J. Am. Chem. Soc. 2014, 136, 6995−7005

toehold-mediated strand displacement.[20] The unfolding process is typically complete in less than half an hour even at room temperature and leads to a yield of almost 100%. Overall, the folding and unfolding kinetics are shown to be well-controllable and reasonably fast, making them useful reconfiguration mechanisms in the inventory of dynamic DNA origami. For example, the flat-to-circular transition can be used to controllably trigger seed-catalyzed DNA tubule growth.[21]

In the field of DNA nanotechnology, there has been growing interest in the mechanical properties of self-assembled DNA structures, which are essentially bundles of DNA double helices interconnected by crossovers. The torsional rigidity of such bundles has been directly measured using magnetic tweezers,[22] and the bending stiffness has also been investigated by cyclization studies[23] or by probing the persistence length via imaging methods.[24] However, the rigidity of the interhelix crossovers, the connecting part, is still largely unknown. As a result, it remains unclear to what extent one helix can rotate about another helix within the assembled structure.[23] Such uncertainty may pose difficulties in predicting the dynamic behavior of DNA nanostructures.

Because of its small length scale, the fluctuation of a single crossover is difficult to monitor experimentally. However, within a typical DNA origami tile, the crossovers are arranged into an ordered array, and their bending can be accumulated to produce observable effects (the cyclization of an origami sheet in this work). From our kinetic study of the tile cyclization process, the activation energy is probed as a function of origami geometry and missing staples. The experimental observations can be well-described by a simple mechanical model that includes the bending flexibility of crossovers. From this model, we estimate that the effective bending stiffness of a phosphate bond in crossovers is similar to that of a one-base-long single-stranded DNA and that crossovers contribute most of the bending flexibility of a DNA origami sheet. This finding advances our understanding of DNA mechanics and should be important for the design and prediction of self-assembled DNA structures.

SCHEME AND MODEL SETUP

In this work, a two-dimensional rectangular DNA origami tile 32 helices in height and 224 bases in width is designed as a model system. A set of linker strands is used to connect the upper and lower edges of the origami, as illustrated in Figure 1a. Here the linkers (shown in red) are arranged parallel to the scaffolds (shown in blue and black). They simultaneously hybridize with the scaffolds on both edges and thus link them. To make the process reversible, we attached eight-base-long toehold segments (shown in green) of random sequences to both the 5′ and 3′ ends of each linker. The releaser strands, which are completely complementary to the linkers, first hybridize with the unpaired toeholds and then completely base-pair with the linkers via branch migration, thereby releasing the linkage. The normal staples on the left and right edges were intentionally removed to prevent blunt end stacking.[1] To allow optical monitoring of the tile conformation, two staples on the upper and lower edges are labeled with 6-carboxyfluorescein (FAM) and tetramethylrhodamine (TAMRA), respectively, which display individual emission signatures peaking at ∼520 and 580 nm. In a folded tile, the FAM and TAMRA labels on opposite edges are brought to close proximity with each other, and efficient Förster resonance energy transfer (FRET) occurs. When the tile unfolds, the FAM donor and TAMRA acceptor are separated, causing a drastic decrease in the FRET efficiency. As a result, the FAM fluorescence at 520 nm is no longer quenched and increases significantly.

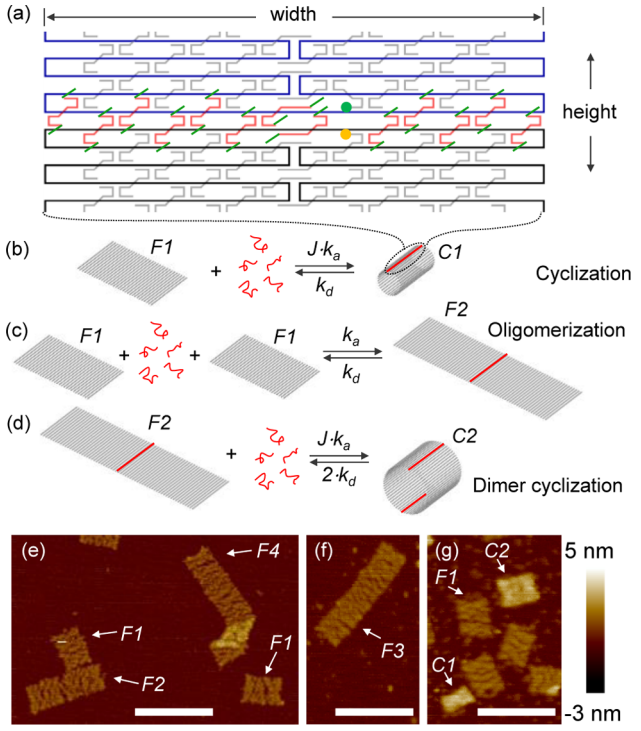

Figure 1. (a) Schematic of a folded scaffold with its opposite edges (black and blue) connected and sealed by a set of toehold-primed linker strands. The linkers and toeholds are shown in red and green, respectively. Staple strands used to construct the origami tiles are shown in gray. The green and yellow dots represent FAM and TAMRA fluorophores. (b–d) Illustration of possible reaction pathways. DNA double helices are presented as gray rods. Red lines represent sealed edges. J, k_a, and k_d are kinetic parameters that govern the reaction rates. (b) Monomer cyclization. A flat origami tile (F1) folds up and cyclizes into a short, cylindrical tube (C1). (c) Dimerization. Two flat monomers react and form a flat dimer (F2). (d) Dimer cyclization. A dimer seals its two edges and cyclizes into a short tube (C2). (e–g) AFM images of various DNA origami species. The identity of each origami is marked in the images. The striated pattern clearly shows the orientation of the DNA strands. The tiles are connected in the direction perpendicular to the DNA strands. The F4 object twisted twice when it adsorbed on the substrate. Scale bar: 200 nm.

Figure 1 also illustrates the typical reaction pathways of the system. A flat origami tile (F1) can fold up and seal into a short hollow tube (C1). Other side reactions include the dimerization of two tiles into a flat dimer (F2) and the cyclization of a dimer into a tube with a larger diameter (C2). Although not illustrated here, even higher order reactions involving more tiles are also possible. The generalized reaction pathways can be divided into two types: cyclization and oligomerization. Cyclization is described by the following reaction:

$$\mathrm{F}n + \mathrm{L} \underset{n \cdot k_d}{\overset{J \cdot k_a}{\rightleftarrows}} \mathrm{C}n \tag{1}$$

Oligomerization can be described by the following reactions:

$$2\mathrm{F}n + \mathrm{L} \underset{k_d}{\overset{k_a}{\rightleftarrows}} \mathrm{F}(2n) \tag{2}$$

$$\mathrm{F}n + \mathrm{F}m + \mathrm{L} \underset{2k_d}{\overset{k_a}{\rightleftarrows}} \mathrm{F}(n+m) \tag{3}$$

dx.doi.org/10.1021/ja500612d | J. Am. Chem. Soc. 2014, 136, 6995–7005

where F and C denote the flat and cyclized origami conformations and n and m denote numbers of monomer tiles that particular DNA assemblies contain. L is used to represent the linker set. J denotes the j factor, an intrinsic property of a cyclizable molecule. It has the unit of nM and can be understood as the effective local concentration of reactive ends: two ends of one molecule are always confined in the vicinity of each other, but the rate of their association depends on the probability of the molecule to bend into correct circular conformation. By serving as a kinetic parameter for the cyclization reaction, the j factor also characterizes the readiness of a molecule to flex over into a circular form. As a result, it is a good indicator of the flexibility and conformation of a molecule.[23,25−27] The reverse reaction involves the breaking of existing linkages. Depending on the specific reaction pathway, the reverse process can be achieved through linkage breaking at one or more sites (see the Supporting Information for details).

Throughout this study, we use the same high linker concentration (200 nM, at least 45 times in excess with respect to the origami monomers) to make linker exhaustion negligible. Therefore, the linker concentration [L] is held nearly constant at all times. Since the linkers are constantly and abundantly available, we treat oligomerization as a second-order bimolecular reaction and cyclization as a first-order unimolecular reaction whose rate can be correlated with the bimolecular reaction rate by the j factor. The forward and reverse reaction rate constants are denoted as k_a and k_d, which have units of $nM^{-1}\ s^{-1}$ and s^{-1}, respectively. As a common assumption, k_a is assumed to be independent of the size of the reacting DNA assembly, and every linkage in one oligomer has equal probability to break with dissociation rate constant k_d. Under such assumptions, the oligomerization rate can be presented as $k_a\cdot[Fn]\cdot[Fm]$. To model the cyclization reaction, we borrow the concept of the j factor (or J) from polymerization theory[28] and DNA cyclization studies.[23,25−27] The j factor is defined by Shore et al.[27] as "the ratio of the equilibrium constants for cyclization and for bimolecular association via the cohesive ends". By this definition, the cyclization rate for species Fn is expressed as $k_a\cdot J\cdot[Fn]$.

In our experiments, we found that the origami species are predominantly monomers (F1 and C1) and dimers (F2 and C2), with some rare F3 and F4 species. Higher-order species such as C3, C4, and F5 were never observed. Therefore, we considered cyclization and oligomerization up to C2 and F4, respectively. The reaction equations can be listed as follows:

$$\mathrm{F1} + \mathrm{L} \underset{k_{d,c}}{\overset{J\cdot k_a}{\rightleftarrows}} \mathrm{C1} \tag{4}$$

$$\mathrm{F2} + \mathrm{L} \underset{2k_{d,c}}{\overset{J_2\cdot k_a}{\rightleftarrows}} \mathrm{C2} \tag{5}$$

$$2\mathrm{F1} + \mathrm{L} \underset{k_{d,f}}{\overset{k_a}{\rightleftarrows}} \mathrm{F2} \tag{6}$$

$$\mathrm{F2} + \mathrm{F1} + \mathrm{L} \underset{2k_{d,f}}{\overset{k_a}{\rightleftarrows}} \mathrm{F3} \tag{7}$$

$$2\mathrm{F2} + \mathrm{L} \underset{k_{d,f}}{\overset{k_a}{\rightleftarrows}} \mathrm{F4} \tag{8}$$

$$\mathrm{F3} + \mathrm{F1} + \mathrm{L} \underset{2k_{d,f}}{\overset{k_a}{\rightleftarrows}} \mathrm{F4} \tag{9}$$

Because oligomers with different sizes often have different values of the j factor, a separate j factor, J_2, is assigned to dimer tiles. Additionally, cyclized species experience more mechanical strain than flat species (see Mechanical Analysis of Elastic Deformation, below). As a result, the linkages in cyclized species may be more prone to break. To be able to examine such an effect, we keep the kinetic model general and assign separate dissociation rate constants to flat and cyclized species, which are denoted as $k_{d,f}$ and $k_{d,c}$ respectively. It is expected that $0 \le k_{d,f} \le k_{d,c}$.

On the basis of the above reaction equations, a set of ordinary differential equations (ODEs) can be developed. We normalized the concentration of every species with the initial concentration of flat monomer, $[F1]_0$. The normalized concentrations are denoted by a bar, and the dimensionless set of ODEs is as follows:

$$\frac{d}{dt}\overline{[C1]} = k_a\cdot[F1]_0\cdot\overline{J}\cdot\overline{[F1]} - k_{d,c}\cdot\overline{[C1]} \tag{10}$$

$$\frac{d}{dt}\overline{[C2]} = k_a\cdot[F1]_0\cdot\overline{J_2}\cdot\overline{[F2]} - 2\cdot k_{d,c}\cdot\overline{[C2]} \tag{11}$$

$$\begin{aligned}\frac{d}{dt}\overline{[F1]} = {} & k_a\cdot[F1]_0\cdot\{-2\cdot\overline{[F1]}^2 - \overline{[F2]}\cdot\overline{[F1]} - \overline{[F3]}\cdot\overline{[F1]} \\ & - \overline{J}\cdot\overline{[F1]}\} + k_{d,f}\cdot\{2\cdot\overline{[F2]} + 2\cdot\overline{[F3]} + 2\cdot\overline{[F4]}\} \\ & + k_{d,c}\cdot\overline{[C1]}\end{aligned} \tag{12}$$

$$\begin{aligned}\frac{d}{dt}\overline{[F2]} = {} & k_a\cdot[F1]_0\cdot\{\overline{[F1]}^2 - \overline{[F2]}\cdot\overline{[F1]} - 2\cdot\overline{[F2]}^2 \\ & - \overline{J_2}\cdot\overline{[F2]}\} + k_{d,f}\cdot\{-\overline{[F2]} + 2\cdot\overline{[F3]} + 2\cdot\overline{[F4]}\} \\ & + 2\cdot k_{d,c}\cdot\overline{[C2]}\end{aligned} \tag{13}$$

$$\begin{aligned}\frac{d}{dt}\overline{[F3]} = {} & k_a\cdot[F1]_0\cdot\{\overline{[F2]}\cdot\overline{[F1]} - \overline{[F3]}\cdot\overline{[F1]}\} \\ & + k_{d,f}\cdot\{-2\cdot\overline{[F3]} + 2\cdot\overline{[F4]}\}\end{aligned} \tag{14}$$

$$\frac{d}{dt}\overline{[F4]} = k_a\cdot[F1]_0\cdot\{\overline{[F2]}^2 + \overline{[F3]}\cdot\overline{[F1]}\} - 3\cdot k_{d,f}\cdot\overline{[F4]} \tag{15}$$

At the onset of the reaction (i.e., at $t = 0$), $\overline{[F1]}$ is equal to 1, while the normalized concentration of every other species is equal to 0. With these initial conditions, the set of ODEs can be numerically solved for a set of floating kinetic parameters (k_a, $k_{d,c}$, $k_{d,f}$, J, and J_2). Residual minimization was performed to extract the kinetic parameters that provide the best agreement between the numerical solution and the experimentally obtained statistical data. Additional constraints were needed to make the parameter extraction robust. Since $0 \le k_{d,f} \le k_{d,c}$, we examined and compared two extreme cases by dictating either $k_{d,f} = 0$ or $k_{d,f} = k_{d,c}$. The further simplification of dictating $J = J_2$ could be made to speed up the minimization process. This simplification did not significantly affect the extracted k_a, $k_{d,c}$, and J values (see Figure S9 in the Supporting Information). All of the conditions yielded generally good agreement and the extraction of similar k_a and J values. The best fit was achieved by using the $k_{d,f} = 0$ constraint and an independent J_2. All of the kinetic curves presented here were obtained from simulations under these conditions.

dx.doi.org/10.1021/ja500612d | J. Am. Chem. Soc. 2014, 136, 6995−7005

EXPERIMENTAL METHODS

Since the concentration of DNA origami tiles is conserved at $[F1]_0$ during the cyclization/oligomerization reaction, the nondimensionalized concentration of one species is simply its mass fraction divided by the total number of tiles. In this work, we statistically estimated the mass fraction by taking atomic force microscopy (AFM) images of a sample and counting the occurrences of each species. Similar to previous reports,[29,30] the relative abundance of a species in an AFM image (or on a mica substrate) was assumed to represent its relative abundance in solution. As shown in Figures S10 and S11, we also verified this assumption by carrying out calibration measurements on standard sample solutions. The reaction kinetics was characterized by measuring species fractions as functions of time. Factors such as temperature, DNA origami tile concentration, and the intrinsic structure of the tiles were studied.

The starting material for the cyclization/oligomerization reaction (i.e., flat DNA origami monomer tiles) was synthesized by annealing 4.2 nM m13mp18 scaffold (New England Biolabs) with 10× staples in TAEM buffer (1× TAE buffer containing 12.5 mM Mg^{2+}, which was kept throughout the study) from 95 to 4 °C at a rate of 1 °C/min in a thermal cycler.

To study the effect of temperature and tile concentration, part of the 4.2 nM tile solution was diluted to 1.3 nM with TAEM buffer. Concentrated linker solution (5.8 μM) was added to the flat tile solution to a final concentration of 200 nM. The mixtures containing 4.2 or 1.3 nM tiles and 200 nM linkers were then divided into 20 μL aliquots and incubated at the designated temperature (35, 40, 45, or 50 °C) in a thermal cycler for the designated time (0.5, 1, 2, 4, or 8 h in the 35, 40, and 45 °C cases; 10 min, 20 min, 0.5 h, 1 h, and 2 h in the 50 °C case). The thermal cycler was programmed to rapidly cool the aliquot to 4 °C when the incubation time was up. The 4.2 nM aliquots were then diluted to 1.3 nM and stored at 4 °C, while the 1.3 nM aliquots were directly stored at 4 °C. Except during incubation and brief exposure to room temperature, the tile solutions were always kept at 4 °C, where no cyclization or oligomerization was observed even after 5 days. The samples of the incubated aliquots were characterized by air-phase AFM. To deposit the DNA structures on a substrate, 20 μL of TAEM buffer was first deposited on freshly cleaved mica, followed by 2 μL of sample solution. The mica substrate was incubated for 10 min in a Petri dish at room temperature and then blown dry with compressed air. The mica disc was immediately washed by depositing 80 μL of washing solution (1:1 ethanol/water mixture[10]) on it and blowing it dry three times. Air-phase AFM was performed with a Dimension Icon atomic force microscopy and a SCANASYST-AIR probe (Bruker). At least three 5 μm × 5 μm AFM images were taken for each measurement. The DNA structures were then identified and counted. The total number of tiles counted for each measurement ranged from 300 to 2000.

To study the effect of origami flexibility and origami geometry, special flat tiles were prepared by eliminating staples from the original complete staple set. To study the effect of isolated missing staples, 7, 14, or 21 nonadjacent staples (at positions illustrated in Figure S4) were intentionally excluded. To study the effect of origami height, 5 or 10 consecutive rows of staples (at positions illustrated in Figure S19) were excluded to produce shorter tiles that were 22 or 12 helices in height. The synthesis of these special tiles was performed in exactly the same way as for the original tile: 4.2 nM scaffold was mixed with 10× staples, and the mixture was annealed and diluted to 1.3 nM. The folding behaviors of these special tiles were examined at 40 °C similarly as the original tiles: 20 μL aliquots containing 1.3 nM tiles and 200 nM linkers were incubated for the designated time and characterized by air-phase AFM.

To visualize the structure details of the origami structures in their most native environment, liquid-phase AFM imaging was also performed for some samples. Sample deposition was achieved by incubating 20 μL of TAEM buffer and 1.6 μL of sample solution on freshly cleaved mica for 5 min. The imaging was performed with a SCANASYST-Fluid+ probe (Bruker).

The reverse unfolding process was also studied in this work. The starting material was highly homogeneous (>90%) folded monomer (C1) solution prepared by annealing 4.2 nM scaffold with 10× staples and 200 nM linkers in one pot (Figure S11d). To enable fluorescence measurements, each tile was decorated with two fluorescently labeled staples (a FRET pair, as shown in Figure 1a), and the free, excess staples were removed by centrifugal filtration (Amicon Ultra-0.5, Ultracel-100 membrane, 100 kDa) five times. The unfolding kinetics was studied by monitoring the decrease in the FRET signal (increase of FAM fluorescence at 520 nm) over time. Fluorescence measurements were performed with a spectrofluorometer (HORIBA Jovin Yvon Fluorolog-3) and a StepOnePlus real-time polymerase chain reaction (RT-PCR) machine, which also measured the melting curve. To account for sample loss during centrifugal filtration, the tile concentration of the filtered sample was redetermined by fluorescence correlation spectroscopy (FCS) (see the Supporting Information for details).

RESULTS

External Parameters That Govern the Reconfiguration Reaction Kinetics. In this study, the starting tile ensembles were highly homogeneous. The flat tile solution (Figure 2a) did not appear to contain any folded species. The one-pot folded solution (represented by Figure 2b) contained over 90% cyclized monomer tiles. The flat origami tiles in Figure 2a measured

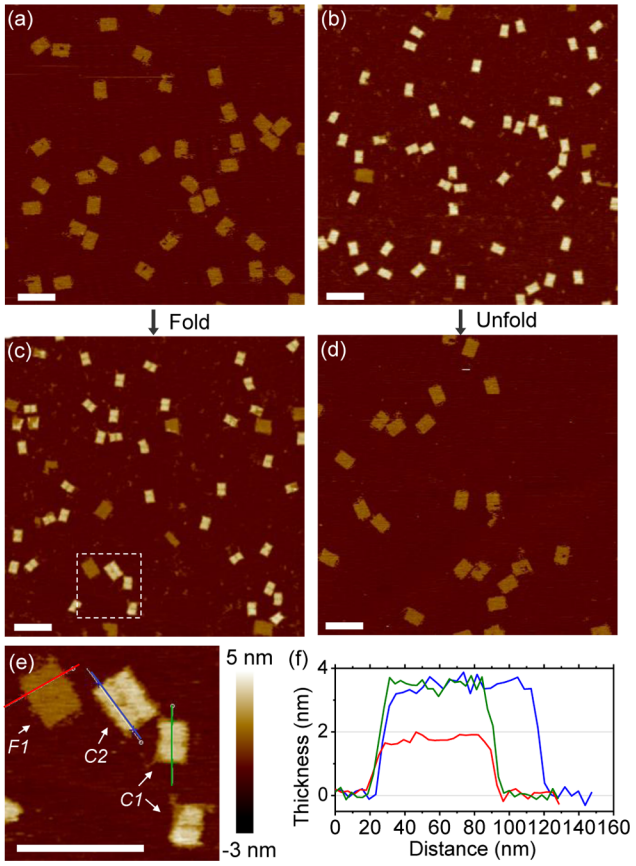

Figure 2. AFM images of the DNA origami species. (a) Near 100% flat origami tiles (F1) prepared by annealing without linkers. (b) Over 90% cyclized origami (C1) prepared by one-pot annealing with linkers. (c) Mixture of species obtained by folding of flat monomers from (a) at 45 °C for 2 h. Multiple F1 and C1 as well as one C2 are present. (d) Nearly 100% F1 generated by unfolding of short tubes from (b) at room temperature. (e) Zoom-in image showing F1, C1, and C2 species excerpted from (c). (f) Cross-section profiles of the three tiles indicated in (e). C1 has exactly the same width as F1. The thicknesses of C1 and C2 are twice that of F1. Scale bars: 200 nm. The original 5 μm × 5 μm AFM images are presented in the Supporting Information.

dx.doi.org/10.1021/ja500612d | J. Am. Chem. Soc. 2014, 136, 6995−7005

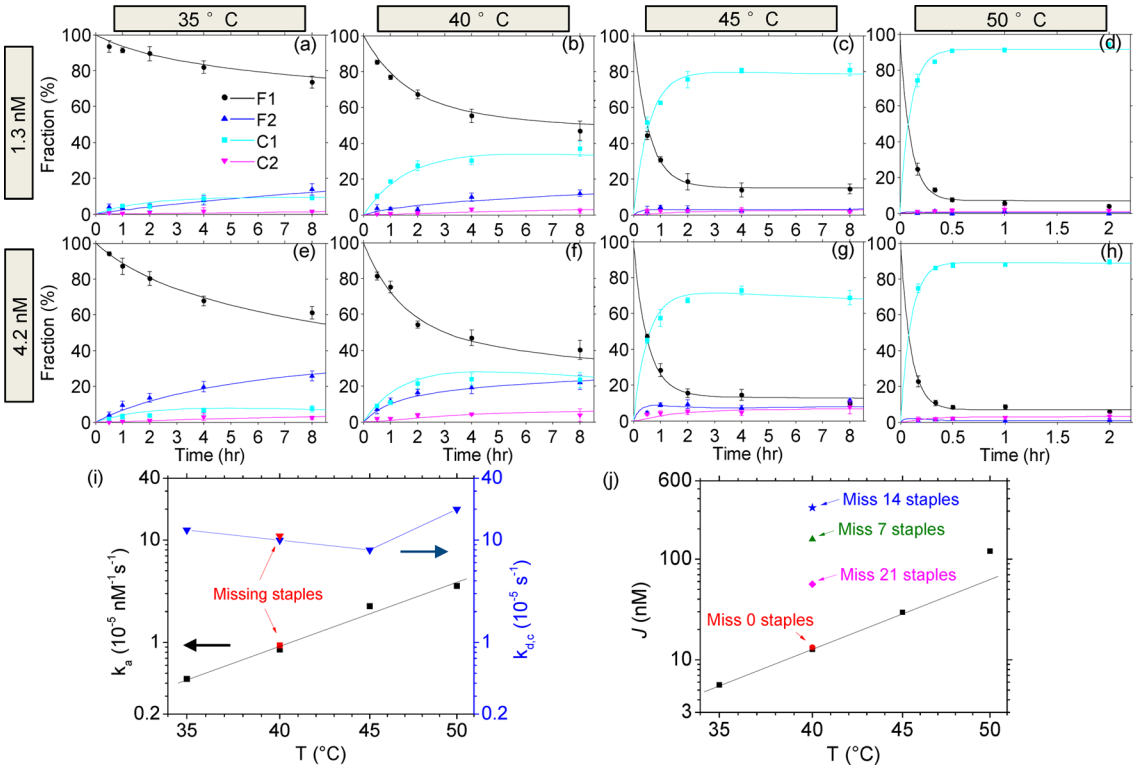

Figure 3. Experimental (solid symbols) and numerical simulation (solid curves) results for the time evolution of the fraction of DNA origami species as a function of incubation temperature and initial monomer concentration. The fractions of origami species were statistically counted over time after the addition of linker strands to initiate structural reconfiguration. (a–d) Fraction evolution from an initial monomer concentration of 1.3 nM at (a) 35, (b) 40, (c) 45, and (d) 50 °C. (e–h) Fraction evolution from an initial monomer concentration of 4.2 nM at (e) 35, (f) 40, (g) 45, and (h) 50 °C. It should be noted that the time scale in the 50 °C cases is different to capture their fast reaction kinetics. (i) Association (black squares) and dissociation (blue triangles) rate constants as functions of temperature. The red symbols of corresponding shape denote the extracted k_a and $k_{d,c}$ values for tiles with 0, 7, 14, and 21 missing staples. Missing staples did not significantly change the two parameters. (j) Monomer *j* factor as a function of temperature extracted from fitting the kinetic model. Black solid squares denote our original design, while the other symbols represent origami samples with 0, 7, 14, or 21 staples excluded. Missing staples increased the structural flexibility of the origami, thus changing the cyclization efficiency or *J*. Note that the kinetic parameters are plotted as functions of temperature instead of the inverse of absolute temperature for clarity. The x-axis is scaled such that the Arrhenius equation plots linearly.

approximately 100 nm in height and 70 nm in width. The short cylindrical tubes formed by sealing the upper and lower edges collapsed into a rectangular shape to maximize their contact with the mica substrate (Figure 2b). The size of the resultant rectangles measured about 70 nm × 50 nm, half that of the flat monomer tiles. The thickness of a folded tile was about 4 nm, twice the thickness of a flat tile (Figure 2e,f). Figure 2c shows a typical AFM image after addition of linker strands. The image was taken after incubation at 45 °C for 2 h, and we observed a mixture of origami species including cyclized monomers and dimers (C1 and C2, respectively) along with unreacted flat monomers (F1). In this case, the cyclized short tubes, C1, took up approximately 70% of all the tiles. When the incubation temperature was increased to 50 °C, the fraction of C1 was measured to be greater than 90%. The unfolding process was efficient even at room temperature (~22 °C). As shown in Figure 2d, all of the origami structures displayed the morphology of F1 30 min after the addition of releaser strands.

The *j* factor of DNA has been shown to depend on temperature.[31] From our reaction model, increased initial tile concentration was also expected to influence the kinetic behavior by shifting the reaction toward the oligomerization pathway. Therefore, we examined the kinetic effect of these two parameters. The fraction of origami species as a function of incubation time was measured under different conditions. Figure 3a–h shows the time evolutions of the fraction of DNA origami species at 35, 40, 45, and 50 °C from two different initial origami concentrations (1.3 and 4.2 nM). The experimental results are plotted as solid symbols; the numerical solutions from our kinetic model are overlaid as solid curves in corresponding colors. Since the fractions of F3 and F4 remained nearly zero throughout all of the experiments, they were not plotted.

The reaction kinetics was accelerated by increasing the incubation temperature, as expected. More importantly, the cyclization yield increased significantly from 10 to 90% when the temperature was elevated from 35 to 50 °C. The end-joining reactions also became more efficient with increasing temperature, as indicated by the decrease in the fraction of unreacted F1 from about 70 to 10%. However, the increased end-joining efficiency did not lead to increases in the fractions of of oligomerized species such as F2 and C2. In fact, the oligomer fractions decreased steadily with increasing temperature. This opposition in trends indicates that the cyclization reaction rate increased faster than the oligomerization rate. As a result, cyclization suppressed oligomerization by rapidly consuming reactive monomer tiles. The >20-fold increase in the *j* factor shown in Figure 3j confirms this qualitative conclusion. In a parallel observation, it is clear that a high initial monomer concentration, $[F1]_0$, favors oligomerization, as oligomerized

dx.doi.org/10.1021/ja500612d | *J. Am. Chem. Soc.* 2014, 136, 6995–7005

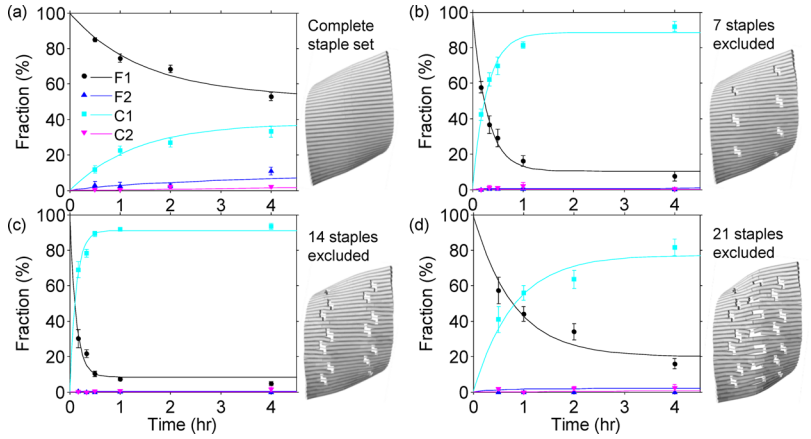

Figure 4. Evolutions of species fractions as functions of time for origami sheets with (a) 0, (b) 7, (c) 14, and (d) 21 staples excluded. Front views of CanDo-simulated origami structures are presented beside the plots for visualization of the effect of eliminating staples. The overall structural shapes were little affected by missing staples.

species were always more abundant in the 4.2 nM case than in the 1.3 nM case.

The agreement between the experimental results and our simulations is fairly good. A set of kinetic parameters (k_a, $k_{d,c}$, J, and J_2) simultaneously describe the time evolutions from the two different initial concentrations with reasonable accuracy. Most data points coincide within the experimental uncertainty margin. The kinetic parameters for the best fit are plotted in Figure 3i,j. The association rate constant k_a follows the Arrhenius equation with good linearity in semilog plots. The activation energy for the association reaction was determined to be 28.7 ± 2.5 kcal/mol. The values of the j factor below 50 °C fit the Arrhenius equation excellently, with an activation energy of 32.4 ± 0.7 kcal/mol. This activation energy represents the energy barrier for bringing the origami rectangle into a correct circular conformation so that the linkers can effectively hybridize with both edges. As will be discussed later, a simple mechanical model can give a good estimation of this energy barrier by modeling the double helices and crossovers as springs.

The J value at 50 °C is significantly larger than that predicted by the Arrhenius equation. This deviation is probably due to the partial dissociation of staples at a high temperature. Yan and co-workers mapped the thermal behavior of DNA origami by functionalizing neighboring staples with FRET dyes and measuring the FRET efficiency as a function of temperature.[32] From their experimental results, the complete dissociation of staples is rare at or below 50 °C. However, partial dissociation may be significant at that temperature. The single-stranded domains resulting from partial dissociation are mechanically much more compliant than double strands. As a result, the overall structure is softened and easier to bend over, leading to the increased j factor. The melting temperature for our tiles was shown to be above 55 °C (Figure S14b). Since the melting of DNA origami happens with a narrow temperature range,[32] we hypothesize that the effect of staple dissociation is not significant at or below 45 °C, which is over 10 °C below the melting temperature. The excellent linearity of the J plot at 35, 40, and 45 °C serves as a confirmation. To accurately extract the activation energy for completely base-paired origami tiles, the 50 °C data point was excluded from the Arrhenius analysis.

While k_a and J closely follow the Arrhenius equation, $k_{d,c}$ ranges around 10^{-4} s^{-1} within a factor of ~2. We hypothesize that $k_{d,c}$ is determined by two parallel processes. First, the cyclized tiles may have a low probability of opening up (i.e., linkage rupture) due to their mechanical strain. This process is relatively insensitive to temperature. Second, the linker strands can spontaneously dissociate even when below the melting temperature. This process is rare at low temperatures but becomes significant at 50 °C. Because of the different temperature dependences of the two processes, $k_{d,c}$ remains nearly constant at low temperatures and increases rapidly at 50 °C.

Effect of Structural Properties. The intrinsic structural stiffness would also be expected to significantly affect the cyclization behavior. To examine this effect, origami reconfiguration under isothermal conditions (40 °C) was performed for origami tiles from which staples were intentionally excluded. Three types of tiles, with 7, 14, and 21 staples removed, were examined alongside the original intact tiles that contained the complete staple set. The positions of the missing staples were sparsely distributed across the rectangular tile so that the resultant single-strand domains were isolated. The finite-element simulation results from CanDo[33,34] presented in Figures 4 and S18 show that the equilibrium global twisting is largely determined by the helix−pitch mismatch and little affected by isolated single-strand "holes". Since the global conformation is largely unchanged, any increase in j factor should primarily correlate with increased origami flexibility rather than conformational change.

Figure 4 shows the time evolutions of the species fractions as functions of the number of missing staples. The four sets of experimental data can be fitted with the same set of k_a, $k_{d,c}$, and J_2. The change in J alone can account for all of the differences in reaction kinetics. The folding kinetics for the intact tile (Figure 4a) was very close to the previously measured result at the same temperature and tile concentration (Figure 3b). In contrast, the kinetics was significantly changed even when only seven staples were eliminated. The monomer j factor increased 12-fold to ~150 nM. The accelerated folding reaction practically reached completion within 1 h, and the final folding yield was over 90%. The reaction was accelerated even more when 14 staples were eliminated, and the reaction reached completion in about 0.5 h. When too many staples (e.g., 21) were eliminated, however, the folding efficiency started to decrease from the highest value, probably because of compromised structural integrity (see the comparison of the AFM images of the four tiles in Figures S12 and S13). The extracted k_a, $k_{d,c}$ and J values are plotted in Figure 3i,j alongside the results of the previous section. It can be seen

dx.doi.org/10.1021/ja500612d | J. Am. Chem. Soc. 2014, 136, 6995−7005

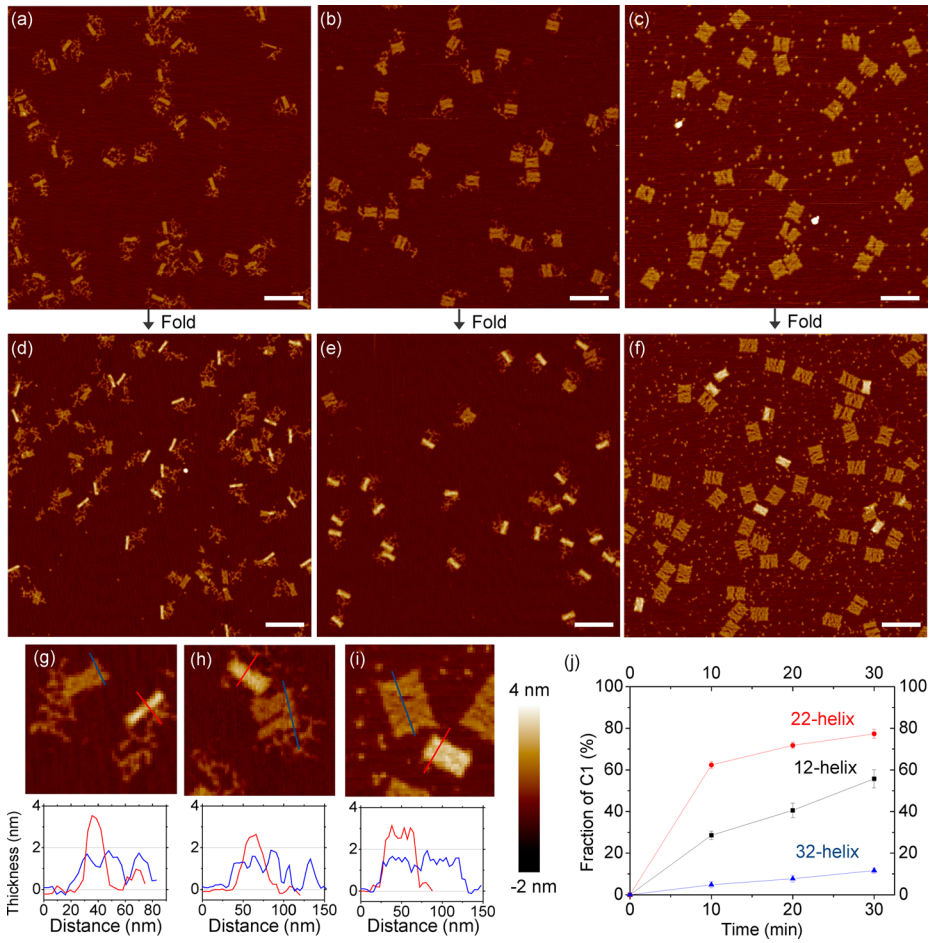

Figure 5. Representative AFM images of flat origami tiles (a–c) before and (d–f) after folding (30 min after addition of linkers). The origami tiles contain 12 helices in (a), (d), and (g), 22 helices in (b), (e), and (h), and 32 helices in (c), (f), and (i). Scale bars: 200 nm. (g–i) Zoom-in AFM images (240 nm × 240 nm) with corresponding cross-section profiles. (j) Fractions of C1 (i.e., folding yields) for different tiles as functions of time.

that k_a and $k_{d,c}$ are hardly affected by the missing staples while J sensitively depends on the number of missing staples.

A high j factor of ~320 nM was achieved when 14 staples were eliminated. Even higher values would be expected if we were to simultaneously exclude staples and increase the incubation temperature. From our reaction model, the fraction of oligomerization products can be limited to <10% when the starting monomer concentration is less than 1/10 of the j factor. In DNA origami studies, the concentration is typically below 10 nM. Therefore, by using rational designs and/or choosing suitable incubation conditions, this folding mechanism can work effectively for typical DNA origami applications without the need for dilution.

Effect of Origami Geometry. To probe the effect of origami geometry, we synthesized shorter origami rectangles (12 and 22 helices in height) by eliminating 10 or 5 consecutive rows of staples from the initial 32-helix rectangle design.[6] New linker sets were designed to bridge the opposite edges of the shorter tiles in exactly the same configuration. The shorter tiles as well as the original one were mixed with 200 nM corresponding linkers and incubated at 40 °C for 10, 20, or 30 min. Figure 5 shows representative AFM images. For the shorter tiles, the unused scaffold segment appears as a random filament beside the distinct rectangular structure. The width of all of the tiles remained at about 70 nm regardless of the tile height or whether the tile was folded. Before folding, the height of the 12-helix tile ranged from 30 to 35 nm, close to the expected value of 35 nm. The height of the 22-helix tile measured from 60 to 65 nm, consistent with the expected value of 65 nm. The height of the 32-helix tile was 100 nm, the same as measured before.

Figure 5d–f shows representative AFM images after 30 min of incubation with linkers. The corresponding zoom-in images and cross-section profiles are presented in Figures 5g–i. While some tiles remain unchanged, distinct new species appear in each image. The new species are about half the height and twice the thickness of the flat tiles, which unambiguously indicates their identity as folded monomers (C1).

The flat and folded tiles in an image can be clearly identified by their difference in size and contrast. After 30 min of incubation, over half of the 12-helix tiles and most of the 22-helix tiles are folded, while only a small portion of the original 32-helix tiles are folded. The exact folding yields as functions of time are presented in Figure 5j. It is unambiguous that the 22-helix tiles have the highest folding reaction rate, while the folding reaction rate of 32-helix tiles is significantly lower than those of the other two types of tile. The nondimensionalized folding reaction rate is $J \cdot k_a$. Since the three types of rectangles use the same linking mechanism, their association rate constants k_a should be close. Therefore, we have the following relation:

$$J(\text{22-helix tile}) > J(\text{12-helix tile}) > J(\text{32-helix tile}) \qquad (16)$$

dx.doi.org/10.1021/ja500612d | J. Am. Chem. Soc. 2014, 136, 6995–7005

Unfolding Process. The unfolding process was found to be kinetically fast even at room temperature. Typical AFM does not have enough temporal resolution to monitor it. Since only one reaction pathway is involved here (no side reactions), we probed the kinetics by monitoring the FRET signals from FAM and TAMRA pairs. Figure 6a shows the fluorescence spectra of the

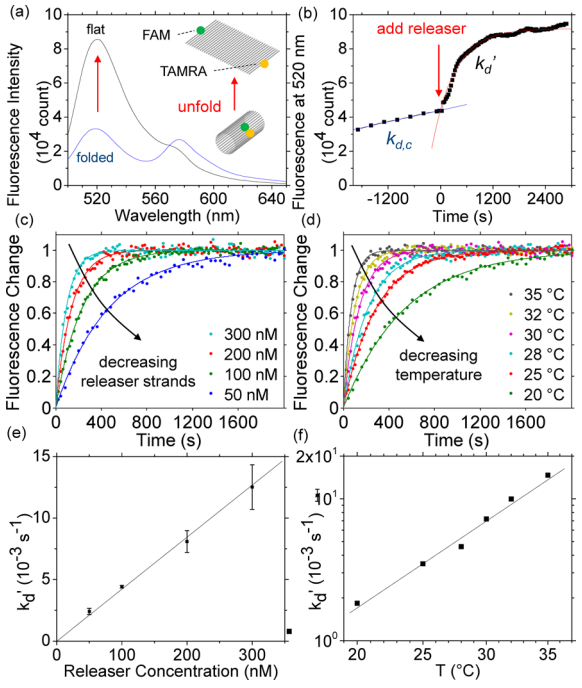

Figure 6. (a) Fluorescence spectra of cyclized (folded) and flat (unfolded) tiles. A FRET pair consisting of FAM ($\lambda_{peak} \approx 520$ nm, shown in green) and TAMRA ($\lambda_{peak} \approx 580$ nm, shown in yellow) indicates the conformation of the DNA origami. When the origami is folded, the FRET signature is evident, as both the FAM and TAMRA signals are distinct, whereas the FAM donor signal is dominant for flat origami. (b) Real-time fluorescence measurements before and after addition of the releaser strands. Black squares, experimental data; blue line, linear fit of the data before addition of releaser strands; red curve, exponential fit of the data after addition of releaser strands. (c, d) Normalized fluorescence changes for (c) various releaser strand concentrations and (d) various incubation temperatures. Circles, experimental data; solid lines, best single-exponential decay fits. (e) Rate constant (k_d') for the unfolding reaction as a function of releaser strand concentration at 30 °C. The error bars were calculated from differences between two measurements. (f) Rate constant for the unfolding reaction as a function of temperature at a releaser strand concentration of 200 nM. Note that the x-axis is scaled to make Arrhenius equation plot linearly.

origami tiles before and after the unfolding reconfiguration. With excitation at 480 nm, FAM fluoresces at ~520 nm, while the TAMRA emission signature exhibits its peak at ~580 nm. The FRET signal is clearly visible for the folded tiles, as the FAM peak intensity is less than 40% of the value in the flat case and the TAMRA signature is much more distinct. In our experiments, the increase in the FAM peak value should be proportional to the amount of F1 species unfolded from C1. The releaser strands were added at least 50 times in excess to make their exhaustion negligible. As a result, the probability for each origami to unfold remained nearly constant, and a single-exponential decay curve was expected for the FAM fluorescence change.

Figure 6b shows the real-time fluorescence measured at 520 nm. When left with no releaser strands at room temperature, the fluorescence intensity of the sample increased slowly with time, indicating the spontaneous unfolding of folded monomers. As a control, flat tile solutions did not show a significant fluorescence change. The unfolding rate can be expressed as $k_{d,c} \cdot [C1]$, where $k_{d,c}$ is the dissociation rate constant for cyclized species as defined before. Because of the efficiency of toehold-mediated strand displacement, the fluorescence increase was dramatically accelerated by the addition of releaser strands. From the slopes of the two fitted functions in Figure 6b, the rate was increased by a factor of 16. We define a new symbol k_d' to denote the dissociation rate constant in the presence of releaser strands. From the fit of the fluorescence curve to an exponential decay function, k_d' can be extracted.

Since the fluorescence increase rate is proportional to the unfolding rate, the dissociation rate constant in the absence of releasers may be calculated as $k_{d,c} = k_d'/16 = 1.2 \times 10^{-4}$ s^{-1}. Previously, our reaction rate model concluded that $k_{d,c}$ remained at about 1×10^{-4} s^{-1} at low temperatures, in good agreement with the directly measured value.

To further study the unfolding kinetics, we measured the unfolding rate constant as a function of temperature and releaser concentration. Figure 6c,d shows the corresponding normalized fluorescence changes as functions of time. All of the experimental curves can be described well by exponential decay functions. The extracted k_d' values are plotted in Figure 6e,f. k_d' is nearly proportional to the releaser concentration and follows the Arrhenius equation closely. The activation energy was determined to be 30.2 ± 1.6 kcal/mol, which is close to the value of 33 kcal/mol measured for branch migration.[35] The overall agreement suggests that the unfolding kinetics is well-governed by that of strand displacement. To control the unfolding kinetics, one may change the toehold length,[20] the concentration of releaser strands, or the incubation temperature.

Mechanical Analysis of Elastic Deformation. In our design, the crossovers are placed periodically with a period of 32 base pairs (bp). If double-stranded helices were to complete one turn every 10.66 bp, the design would result in a planar origami sheet. However, the helical pitch of unstrained B-form DNA in solution is approximately 10.5 bp.[36,37] The slight difference causes the origami to assume a twist-bend curvature,[32,33] as shown in Figure 7a.

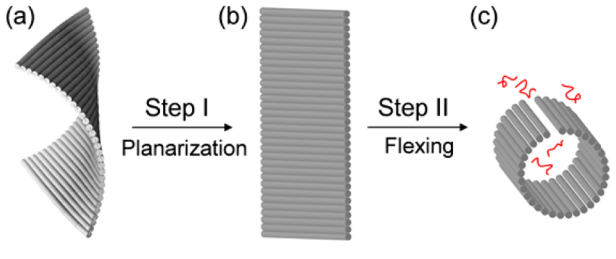

Figure 7. Schematic illustration of the conceptual two-step folding process: (a) equilibrium curved origami sheet; (b) intermediate planar origami sheet; (c) flexed-up origami ready for linker hybridization.

The folded short tube after the addition of linkers is illustrated in Figure 7c. In view of the rotational symmetry of the structure, the double helices in the bundle should be straight and parallel to each other. Consequently, neighboring crossovers on the same double helix are expected to have identical orientations. Therefore, the double helix should complete an integer number of turns between crossovers. Since the crossover period is still 32

dx.doi.org/10.1021/ja500612d | J. Am. Chem. Soc. 2014, 136, 6995−7005

bp as in our original design, the helical pitch is forced to have a value of 10.66 bp/turn in the folded short tube.

The correct orientation of reactive ends is important for cyclization reactions,[25] and the twist-bend curvature in Figure 7a is expected to inhibit the linker set from working effectively because even if the sheet is deformed to a large extent, the two edges will still have lateral dislocation and the two corresponding binding sites for a linker will still be too far apart. For the linkers to effectively seal the two edges, the edge helices need to be correctly aligned and brought into close proximity. To account for this requirement, we modeled the folding process by conceptually introducing an intermediate planar conformation (Figure 7b). The correct edge alignment can be guaranteed when such a planar sheet is flexed. The folding process can then be divided into two steps:

I. planarize the origami tile from the curved sheet;
II. flex the planar sheet into a closed form for sealing of the two opposite edges.

Step I may be achieved by simply forcing the DNA double helices into a 10.66 bp/turn pitch. As per our design, the origami sheet will then assume a planar conformation. This step requires an energy denoted as E_1. For a 32-helix tile, E_1 = 25.6 kcal/mol (see the Supporting Information for calculation details).

Step II requires the flat origami to be flexed out of plane and into a circular conformation. The bending flexibility of the planar origami originates from two sources, as illustrated in Figure 8.

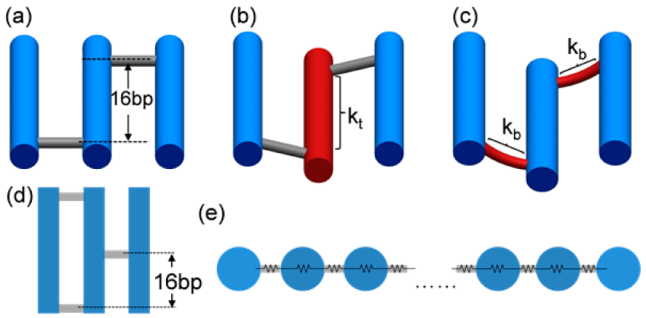

Figure 8. (a) Three-dimensional view of the undeformed structural motif. Blue rods represent double-stranded helices. Gray rods denote crossovers. (b) Twisting of the 16 bp domain between opposite crossovers moves neighboring double helices out of plane. This flexibility is denoted by a torsional spring constant, k_t. The red color highlights the deformed element. (c) Bending of crossovers also moves neighboring double helices out of plane. This flexibility is denoted by a bending spring constant, k_b. (d) Top view of the structural motif in DNA origami. (e) Side view of the equivalent spring network for a planar tile in our mechanical analysis.

First, the crossovers to adjacent rows are arranged in a staggered manner with a distance of 16 bp (Figure 8a,d). The twist of the 16 bp double-stranded helix between opposite crossovers sends adjacent helices out of plane (Figure 8b). Second, a crossover between double helices consists of two phosphate bonds (or only one if the crossover is located on the edge) possessing certain bending flexibility. Bending of the crossovers would flex the sheet further out of plane, as shown in Figure 8c. These flexible components can be modeled as springs connected into a network (Figure 8d,e) whose effective spring constant may be calculated from formulas for springs in parallel and series.[38] Collectively, these flexible joints can create a global flexure of 360°. This step requires an energy denoted as E_2.

To calculate the total energy needed for cyclization, we used the default modulus values from CanDo[33,34] (see the Supporting Information for details). This set of rigidity values is compatible with previous DNA mechanics studies[39−41] and has provided good predictions of three-dimensional origami equilibrium geometry validated by transmission electron microscopy (TEM).[34] To the best of our knowledge, there have been no reports on the rigidity of crossovers. Therefore, we treated this as an unknown parameter to be fixed by our experimental observations.

By adding E_1 and E_2 from steps I and II, we calculated the total elastic energy as a function of origami height, as plotted in Figure 9 (see the Supporting Information for detailed calculations). The

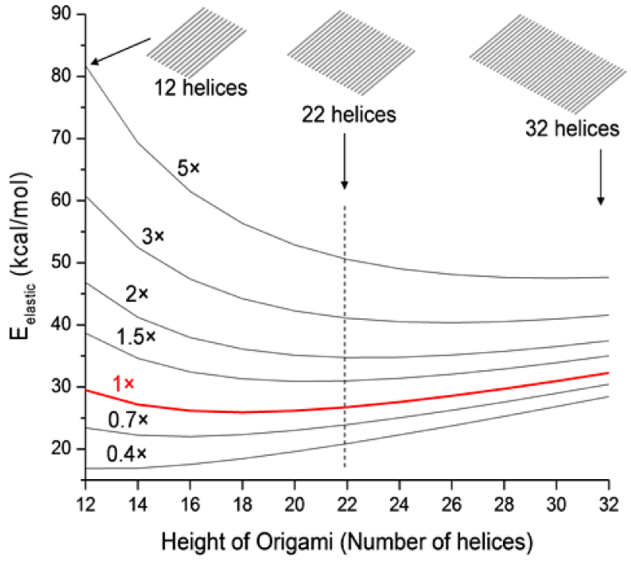

Figure 9. Calculated total elastic energy for bringing an origami tile into circular conformation as a function of origami height. The number near each curve denotes the crossover bending modulus used to calculate that curve, relative to the value for single-stranded DNA.

bending rigidity of the crossover was varied from 0.4 to 5 times that of one-base-long single-stranded DNA. For a longer origami tile of the same width, there are more double helix domains whose helical pitches must be forced to take the value 10.66 bp/turn, and therefore, E_1 increases. However, a longer tile has more flexible joints in series and is easier to flex, resulting in a reduced E_2. If the crossovers are highly flexible, E_1 dominates and the total energy increases with the origami height (e.g., the curve marked as 0.4× in Figure 9). In contrast, if the crossovers are highly rigid, E_2 dominates and the total energy decreases with increasing origami height (e.g., the curve marked 5× in Figure 9). When the crossover rigidity is between these extremes, E_1 and E_2 are comparable. A minimal elastic energy occurs for origami tiles of moderate height. From our experiment, we found the relation in 16, which leads to

$$E_{elastic}(32\text{-helix}) > E_{elastic}(12\text{-helix}) > E_{elastic}(22\text{-helix})$$

This inequality can be satisfied only when the bending stiffness of a phosphate bond in a crossover is within a narrow range around 1 times that of the one-base-long single-stranded DNA (the curve shown in red in Figure 9). Therefore, we estimate that the bending modulus of a crossover phosphate bond is similar to that of single-stranded DNA. Correspondingly, the effective bending spring constant for the bond is 6.8 pN·nm/rad (see the

dx.doi.org/10.1021/ja500612d | J. Am. Chem. Soc. 2014, 136, 6995−7005

Supporting Information for details). From this stiffness value, E_2 was calculated to be 6.7 kcal/mol. The total elastic energy needed to fold a 32-helix origami is 32.3 kcal/mol, which is very close to the experimentally derived value of ~32.4 kcal/mol.

The mechanical model also predicts the effect of missing staples. When some staples are eliminated, the number of double-helix domains to be forced to have a pitch of 10.66 bp/turn in step I decreases, leading to reduced E_1. The origami also becomes more flexible, as there are fewer parallel springs in the spring network. These effects collectively result in a decreased energy barrier and an increased j factor. As an example, we consider the origami tile with seven staples eliminated. The decrease in the energy barrier is calculated to be

$$\Delta E_{\text{elastic}} = -1.51 \text{ kcal/mol}$$

At 40 °C, the j factor is expected to increase by a factor of

$$\exp(-\Delta E_{\text{elastic}}/k_{\text{B}}T) = 11$$

in excellent agreement with the 12-fold increase observed experimentally.

DISCUSSION

Flexibility of Crossovers. Since the crossovers consist of two phosphate bonds and the two bonds are not joined by base recognition at their ends, it is not surprising that the bond's bending flexibility is in a range similar to that of single-stranded DNA.

At least two effects influence the apparent crossover bending flexibility we observed in this work. First, the bending is likely to be a nonlinear process. When the crossovers are significantly bent, electrostatic and steric repulsion between the helices they connect increases rapidly. This effect tends to decrease the apparent crossover flexibility. Second, crossovers create nicks in the double helices they connect. These nicks tend to reduce the local stiffness of the structure and may increase the apparent flexibility of crossovers. For our model system, the two effects seem to offset each other. As a result, the phosphate bond behaves like that in single-stranded DNA.

The flexibility of the origami tile mostly originates from crossover flexibility. When we assumed very large spring constants in the mechanical model for crossovers, thereby eliminating their flexibility, E_2 increased dramatically from 6.7 to 51 kcal/mol. This result indicates that crossovers contribute most of the bending flexibility of the origami tile.

Activation Energy for Cyclization. We experimentally observed a sharp temperature dependence of the cyclization efficiency, corresponding to large activation energy of ~32 kcal/mol. Such a large value can be expected for the folding of macromolecules such as DNA origami or protein.[42] The linkers we used to connect the origami edges bind to one edge of the origami through a 24-base domain and to the other through an eight-base domain. When the origami sheet folds into a short tube, every linker strand contributes an additional 8 bp double helix. According to the nearest-neighbor model,[43] the average decrease in free enthalpy for an 8 bp double helix is 8.8 kcal/mol in 1 M Na^+ at 40 °C. The 13-linker set thus decreases the free enthalpy by ~114 kcal/mol, which is more than enough to compensate for the energy barrier. If the number of linkers is reduced to four, the additional base pairing can only decrease free enthalpy by ~35.2 kcal/mol, which is barely enough to overcome the energy barrier. In view of the fact that the binding between DNA strands is weaker in 12.5 mM Mg^{2+} than in 1 M Na^+,[44] at least five or six linkers are needed for effective folding of our tile under 40 °C. Experimentally, we observed that folded species started to appear when the number of linkers was increased to six (Figure S16). The general agreement provides another confirmation of our analysis.

Activation Energy for End Association. The ~29 kcal/mol activation energy for the end-association reaction between tiles is also quite large. This may explain the relatively ineffective linking in the vertical direction (in our design, the double helices are oriented horizontally). When connecting the tiles vertically, we have never observed origami chains longer than four tiles (~400 nm). In contrast, connecting the tiles horizontally can easily produce ribbons longer than 1 μm (~14 tiles; Figure S15d). Sugiyama and co-workers have also observed a lower linking yield for connecting origami tiles vertically compared with horizontally.[45] Interestingly, the activation energy for vertical end association (29 kcal/mol) is similar to E_1 (25.6 kcal/mol), the energy needed to planarize the tile. We speculate that the linking inefficiency in the vertical direction may be largely due to the inhibitory effect of global twisting. Since the linkers are farther apart in the vertical linking scheme than in the horizontal linking scheme (distance between linkers: ~10 nm vs ~5 nm, respectively), they may be more sensitive to the misalignment between binding sites caused by curved edges.

Guidelines for Designing Dynamic Origami Structures That Use Crossover Flexibility. Our experimental results have demonstrated efficient folding/unfolding origami reconfiguration. For future applications of this reconfiguration mechanism, our mechanical model can provide a few design guidelines based on estimates of the energy barrier:

(1) A minimum number of linkers is required. Because the energy barrier is relatively large (typically >20 kcal/mol), a minimum number of linkers is needed to compensate for it. Our mechanical model can be adapted to calculate the elastic energy barrier for folding of an origami sheet and thereby estimate the minimum number of linkers. To enhance the reaction kinetics and to account for any estimation uncertainty, additional linkers are recommended to effectively drive the folding process.

(2) The energy barrier should be lowered by reducing the global twist of the origami tile. From our calculations, E_1 contributes about three-fourths of the cyclization energy barrier. This portion of the energy barrier has little dependence on the aspect ratio of the origami tile. Therefore, the global twist poses a major obstacle for origami tile folding. Fortunately, the global twist can be reduced by rational design.[30,36] Designs that follow the natural 10.5 bp/turn helical pitch are expected to have a much higher reconfiguration efficiency.

CONCLUSIONS

We have studied the folding and unfolding kinetics of a rectangular DNA origami tile, which represents an alternative mechanism for dynamic shape-changing DNA origami. The folding process utilizes the intrinsic flexibility of an origami sheet and is driven by linkers that connect the two opposite edges. Eliminating a few staple strands or increasing the incubation temperature resulted in folding yields of over 90% within 1 h. The folding process can also be efficiently reversed via toehold-mediated strand displacement.

A simple chemical reaction model has been proposed to describe the cyclization/oligomerization kinetics during the folding reconfiguration. The reaction parameters, such as the association rate constant and j factor, were extracted from the numerical calculations. A two-step mechanical model has been created to correlate microscopic origami structure details with

the observed kinetic behavior. The bending rigidity of DNA interhelix crossovers has been estimated for the first time, and they have been shown to resemble one-base-long single-stranded DNA. Our mechanical model also provides estimates of the energy barrier for origami reconfiguration that should be useful in designing dynamic DNA assemblies. Overall, this study has demonstrated an effective reconfiguration mechanism for DNA origami and elucidated the dynamics of this process. The new reconfiguration mechanism and understanding of DNA mechanical properties should be valuable to the field of DNA nanotechnology.

■ ASSOCIATED CONTENT

Supporting Information

Experimental details and additional data. This material is available free of charge via the Internet at http://pubs.acs.org.

■ AUTHOR INFORMATION

Corresponding Author

jchoi@purdue.edu

Notes

The authors declare no competing financial interest.

■ ACKNOWLEDGMENTS

This research was supported by the U.S. Office of Naval Research (ONR Grants N000141110220 and N00014120829) and the National Science Foundation (NSF Grants 1334088 and 1249315). J.H.C. gratefully acknowledges an NSF CAREER Award.

■ REFERENCES

(1) Rothemund, P. W. K. *Nature* **2006**, *440*, 297.
(2) Jin, Z.; Sun, W.; Ke, Y.; Shih, C.-J.; Paulus, G. L. C.; Wang, Q. H.; Mu, B.; Yin, P.; Strano, M. S. *Nat. Commun.* **2013**, *4*, No. 1663.
(3) Pinheiro, A. V.; Han, D.; Shih, W. M.; Yan, H. *Nat. Nanotechnol.* **2011**, *6*, 763.
(4) Voigt, N. V.; Tørring, T.; Rotaru, A.; Jacobsen, M. F.; Ravnsbæk, J. B.; Subramani, R.; Mamdouh, W.; Kjems, J.; Mokhir, A.; Besenbacher, F.; Gothelf, K. V. *Nat. Nanotechnol.* **2010**, *5*, 200.
(5) Steinhauer, C.; Jungmann, R.; Sobey, T. L.; Simmel, F. C.; Tinnefeld, P. *Angew. Chem., Int. Ed.* **2009**, *48*, 8870.
(6) Fu, Y. M.; Zeng, D. D.; Chao, J.; Jin, Y. Q.; Zhang, Z.; Liu, H. J.; Li, D.; Ma, H. W.; Huang, Q.; Gothelf, K. V.; Fan, C. H. *J. Am. Chem. Soc.* **2013**, *135*, 696.
(7) Pal, S.; Varghese, R.; Deng, Z.; Zhao, Z.; Kumar, A.; Yan, H.; Liu, Y. *Angew. Chem., Int. Ed.* **2011**, *50*, 4176.
(8) Bui, H.; Onodera, C.; Kidwell, C.; Tan, Y.; Graugnard, E.; Kuang, W.; Lee, J.; Knowlton, W. B.; Yurke, B.; Hughes, W. L. *Nano Lett.* **2010**, *10*, 3367.
(9) Endo, M.; Yang, Y.; Emura, T.; Hidaka, K.; Sugiyama, H. *Chem. Commun.* **2011**, *47*, 10743.
(10) Hung, A. M.; Micheel, C. M.; Bozano, L. D.; Osterbur, L. W.; Wallraff, G. M.; Cha, J. N. *Nat. Nanotechnol.* **2010**, *5*, 121.
(11) Kuzyk, A.; Schreiber, R.; Fan, Z.; Pardatscher, G.; Roller, E.-M.; Hoegele, A.; Simmel, F. C.; Govorov, A. O.; Liedl, T. *Nature* **2012**, *483*, 311.
(12) Shen, X.; Asenjo-Garcia, A.; Liu, Q.; Jiang, Q.; García de Abajo, F. J.; Liu, N.; Ding, B. *Nano Lett.* **2013**, *13*, 2128.
(13) Ko, S. H.; Du, K.; Liddle, J. A. *Angew. Chem., Int. Ed.* **2013**, *52*, 1193.
(14) Andersen, E. S.; Dong, M.; Nielsen, M. M.; Jahn, K.; Subramani, R.; Mamdouh, W.; Golas, M. M.; Sander, B.; Stark, H.; Oliveira, C. L. P.; Pedersen, J. S.; Birkedal, V.; Besenbacher, F.; Gothelf, K. V.; Kjems, J. *Nature* **2009**, *459*, 73.
(15) Douglas, S. M.; Bachelet, I.; Church, G. M. *Science* **2012**, *335*, 831.
(16) Kuzuya, A.; Sakai, Y.; Yamazaki, T.; Xu, Y.; Komiyama, M. *Nat. Commun.* **2011**, *2*, No. 449.
(17) Chen, H. R.; Cha, T.-G.; Pan, J.; Choi, J.-H. *Nanotechnology* **2013**, *24*, No. 435601.
(18) Zhang, F.; Nangreave, J.; Liu, Y.; Yan, H. *Nano Lett.* **2012**, *12*, 3290.
(19) Shen, X. B.; Song, C.; Wang, J. Y.; Shi, D. W.; Wang, Z. A.; Liu, N.; Ding, B. Q. *J. Am. Chem. Soc.* **2012**, *134*, 146.
(20) Zhang, D. Y.; Winfree, E. *J. Am. Chem. Soc.* **2009**, *131*, 17303.
(21) Mohammed, A. M.; Schulman, R. *Nano Lett.* **2013**, *13*, 4006.
(22) Kauert, D. J.; Kurth, T.; Liedl, T.; Seidel, R. *Nano Lett.* **2011**, *11*, 5558.
(23) Sa-Ardyen, P.; Vologodskii, A. V.; Seeman, N. C. *Biophys. J.* **2003**, *84*, 3829.
(24) Schiffels, D.; Liedl, T.; Fygenson, D. K. *ACS Nano* **2013**, *7*, 6700.
(25) Podtelezhnikov, A. A.; Mao, C. D.; Seeman, N. C.; Vologodskii, A. *Biophys. J.* **2000**, *79*, 2692.
(26) Koo, H. S.; Drak, J.; Rice, J. A.; Crothers, D. M. *Biochemistry* **1990**, *29*, 4227.
(27) Shore, D.; Langowski, J.; Baldwin, R. L. *Proc. Natl. Acad. Sci. U.S.A.* **1981**, *78*, 4833.
(28) Jacobson, H.; Stockmayer, W. H. *J. Chem. Phys.* **1950**, *18*, 1600.
(29) Jungmann, R.; Scheible, M.; Kuzyk, A.; Pardatscher, G.; Castro, C. E.; Simmel, F. C. *Nanotechnology* **2011**, *22*, No. 275301.
(30) Woo, S.; Rothemund, P. W. *Nat. Chem.* **2011**, *3*, 620.
(31) Geggier, S.; Kotlyar, A.; Vologodskii, A. *Biophys. J.* **2011**, *100*, 76.
(32) Wei, X.; Nangreave, J.; Jiang, S.; Yan, H.; Liu, Y. *J. Am. Chem. Soc.* **2013**, *135*, 6165.
(33) Castro, C. E.; Kilchherr, F.; Kim, D. N.; Shiao, E. L.; Wauer, T.; Wortmann, P.; Bathe, M.; Dietz, H. *Nat. Methods* **2011**, *8*, 221.
(34) Kim, D. N.; Kilchherr, F.; Dietz, H.; Bathe, M. *Nucleic Acids Res.* **2012**, *40*, 2862.
(35) Reynaldo, L. P.; Vologodskii, A. V.; Neri, B. P.; Lyamichev, V. I. *J. Mol. Biol.* **2000**, *297*, 511.
(36) Li, Z.; Liu, M. H.; Wang, L.; Nangreave, J.; Yan, H.; Liu, Y. *J. Am. Chem. Soc.* **2010**, *132*, 13545.
(37) Dietz, H.; Douglas, S. M.; Shih, W. M. *Science* **2009**, *325*, 725.
(38) Timoshenko, S.; Goodier, J. *Theory of Elasticity*; McGraw-Hill: New York, 1987.
(39) Bustamante, C.; Bryant, Z.; Smith, S. B. *Nature* **2003**, *421*, 423.
(40) Strick, T.; Bensimon, D.; Croquette, V. *Genetica* **1999**, *106*, 57.
(41) Wang, M. D.; Yin, H.; Landick, R.; Gelles, J.; Block, S. M. *Biophys. J.* **1997**, *72*, 1335.
(42) Curnow, P.; Booth, P. J. *Proc. Natl. Acad. Sci. U.S.A.* **2009**, *106*, 773.
(43) SantaLucia, J. *Proc. Natl. Acad. Sci. U.S.A.* **1998**, *95*, 1460.
(44) Owczarzy, R.; Moreira, B. G.; You, Y.; Behlke, M. A.; Walder, J. A. *Biochemistry* **2008**, *47*, 5336.
(45) Rajendran, A.; Endo, M.; Katsuda, Y.; Hidaka, K.; Sugiyama, H. *ACS Nano* **2011**, *5*, 665.